Better band gaps with asymptotically corrected local exchange potentials

Prashant Singh,[1,*] Manoj K. Harbola,[2,†] M. Hemanadhan,[2,‡] Abhijit Mookerjee,[3,§] and D. D. Johnson[1,4,‖]

[1]*Ames Laboratory, U.S. Department of Energy, Iowa State University, Ames, Iowa 50011-3020, USA*

[2]*Department of Physics, Indian Institute of Technology, Kanpur 208016, India*

[3]*S. N. Bose National Centre for Basic Sciences, Salt Lake, Kolkata 700098, India*

[4]*Materials Science & Engineering, Iowa State University, Ames, Iowa 50011-2300, USA*

We formulate a spin-polarized van Leeuwen and Baerends (vLB) correction to the local density approximation (LDA) exchange potential [R. van Leeuwen and E. J. Baerends, Phys. Rev. A **49**, 2421 (1994)] that enforces the ionization potential (IP) theorem following T. Stein *et al.* [Phys. Rev. Lett. **105**, 266802 (2010)]. For electronic-structure problems, the vLB correction replicates the behavior of exact-exchange potentials, with improved scaling and well-behaved asymptotics, but with the computational cost of semilocal functionals. The vLB + IP correction produces a large improvement in the eigenvalues over those from the LDA due to correct asymptotic behavior and atomic shell structures, as shown in rare-gas, alkaline-earth, zinc-based oxides, alkali halides, sulfides, and nitrides. In half-Heusler alloys, this asymptotically corrected LDA reproduces the spin-polarized properties correctly, including magnetism and half-metallicity. We also consider finite-sized systems [e.g., ringed boron nitride ($B_{12}N_{12}$) and graphene (C_{24})] to emphasize the wide applicability of the method.

I. INTRODUCTION

Density functional theory (DFT) [1–4] is the most widely used method to explore electronic binding in materials and uses approximate functionals for exchange-correlation (XC) energy calculation. Foremost among them is the local density approximation (LDA) [5], which, over the years, has been improved substantially by developing generalized gradient-corrected approximation (GGA) functionals [6,7]. While these functionals have been quite successful in predicting a large number of properties and are used widely for large systems (due to their computational efficiency and reasonable accuracy), almost all semilocal functionals fail measurably in predicting the correct band gaps. Attempts have been made to improve band-gap prediction using semilocal approaches, such as the self-interaction correction method [8–10] and DFT plus Hubbard corrections (DFT + U) [11]. Other commonly used approaches are the GW approximation [12–17] and hybrid functionals [18,19]. However, they are often limited to small system sizes due to their large computational demand. One significant reason for the partial failure of semilocal XC potentials is their inability to describe the correct asymptotic behavior [10], leading to qualitatively incorrect results for properties sensitive to the asymptote, e.g., the fundamental gap [20–23] and ionization potential (IP) [24].

The poor band-gap predictions in solids using semilocal functionals is understood to arise from the failure to describe correctly the discontinuous jump $\Delta_{\rm xc}$ (a constant) in the Kohn-Sham (KS) potential as the electron number crosses an integer value [20–23,25]. From the continuity of KS orbitals across this jump [20–23,25], it directly follows that $\Delta_{\rm xc} = E_g - E_g^{\rm KS}$, where the fundamental gap ($E_g \equiv I - A$) is the difference between the ionization potential, I, and the electron affinity, A, while the KS gap ($E_g^{\rm KS} \equiv \epsilon_{\rm LU} - \epsilon_{\rm HO}$) is the difference between the lowest-unoccupied (LU) and the highest-occupied (HO) eigenvalues. Any error in $\Delta_{\rm xc}$ (including asymptotic behavior) leads to a large deviation from the IP theorem and underestimation of E_g [20–23,25]. Exact-exchange (EXX) functionals possess $\Delta_{\rm xc}$ by construction [1,26,27]. Kotani implemented EXX in the KS framework for solids and showed substantial improvement in the E_g and asymptotic behavior of the potential [28]. Following this, many attempts were made to mimic EXX behavior with semilocal functionals [29–33]. The van Leeuwen–Baerends (vLB) correction to the LDA exchange used for atoms is one such approach; orbital eigenenergy differences calculated using this approach are close to atomic excitation energies [34–36].

Recently, Kraisler and Kronik [25] showed that all XC functionals (local, semilocal, and nonlocal) generally possess a nonzero $\Delta_{\rm xc}$ and addressed the estimation of E_g within approximate density functionals from ensemble considerations. For finite systems (including small periodic cells) they showed that the $\Delta_{\rm xc}$ from semilocal functionals dramatically improves the predicted E_g, even for the LDA; however, as the system is extended (i.e., large supercells), the ensemble correction for the LDA vanishes. The main difficulty arises because the HO and LU orbitals are delocalized, whereas the XC kernel is very localized in semilocal cases. To avoid addressing the highly nonlocal kernels, an alternative is to localize the HO and LU orbitals, such as by dielectric screening [37], self-interaction correction, or use of small cells (an uncontrolled localization). An alternative is to impose the asymptotic behavior in a solid locally as part of the electronic-structure method, as is easily implemented in site-centered basis-set methods using vLB correction for solids.

*prashant@ameslab.gov

†mkh@iitk.ac.in

‡Present address: Département de Chimie Moléculaire, Université Joseph Fourier, 38041 Grenoble Cedex 9, France.

§abhijit.mookerjee61@gmail.com

‖ddj@ameslab.gov

Using the Harbola-Sahni (HS) exchange potential [38] and vLB correction [34], we have previously established that correcting the asymptotic limits of the exchange potential leads to a significant improvement in the semiconductor band gaps [39,40]. Here, the vLB-corrected LDA [34] is much easier to apply because it can be written in terms of the system density. The vLB correction [34] is constructed along the lines of the Becke functional [41] and makes the XC potential go asymptotically as $-1/r$ "far" from the atom center but still inside the crystal, which must be the local interstitial region surrounding each atom in the solid and which also defines the local crystal potential 0 (to solve accurately the microscopic electrostatics). This approach may be connected (Sec. II B) to range-separated functionals that invoke the asymptotic condition $-1/(\epsilon r)$ involving the dielectric function (ϵ) of the solid [43–45].

In this paper, we implement a spin-polarized version of the vLB correction to the short-range part of the LDA exchange, which is similar to the modified LDA [31], rather than the full range addressed in range-separated hybrid functionals [43–45]. We apply it to a wide range of materials with varying crystal structures, e.g., rare-gas solids, nitrides, oxides, sulfides, ternary half-Heusler alloys, and some finite-size systems. In particular, we address wurtzite-ZnO, spin-polarized, half-Heusler ($C1_b$) FeMnSb, and two-dimensional boron-nitride ($B_{12}N_{12}$). Our spin-polarized vLB-corrected LDA corrects both extreme limits of the potential, i.e., $r \to 0$ and $r \to \infty$, and uses the optimized vLB parameter to obey the IP theorem [20,21,42] for isolated atoms and diatoms; these combined corrections give a substantial improvement in the semiconductor band gaps over the LDA and are similar to the EXX results.

II. BACKGROUND

A. Ionization potential theorem

Perdew *et al.* [20] have shown that for the case of exact KS theory in DFT, the highest-occupied KS eigenvalue is equal and opposite to the ionization potential. Stein *et al.* [46] followed the queue from the IP theorem [20,21,42] to determine the optimal value of the system-independent parameter γ [47] used to evaluate the XC part of their calculation and successfully extended the quantitative usage of DFT for calculating fundamental gaps in finite and bulk systems, a largely unexplored area [44–46].

Hemandhan *et al.* [48] combined the idea of Stein *et al.* [46] with IP theory [20,21,42] to determine the optimal value of β used in the vLB correction term [34]. The vLB correction to LDA exchange implemented with the Vosko-Wilk-Nusair parametrized correlation [49] to calculate the excitation energies of atoms and diatoms following IP theory. To make the optimal choice of β and determine the highest-occupied molecular orbital (HOMO) energies, we enforce Koopmans theorem, i.e., β is varied until the HOMO eigenvalue $\epsilon_{\max}$ and ionization energy match [48], i.e.,

$$\epsilon^{\beta}_{\max} = E(N,\beta) - E(N-1,\beta) = -I^{\beta}(N). \tag{1}$$

Here, N is the number of electrons in the system, $I^{\beta}(N)$ is the energy difference between the ground-state energy of the N and that of the $(N-1)$ electron system per β, i.e., the ionization potential.

B. van Leeuwen–Baerends correction

To apply KS-DFT to a system of interest, we need to approximate the XC potential as accurately as possible in evaluating the effective potential. This potential is largely evaluated by taking the derivative of the XC energy functional, but the system density can also be used to model them directly. Recent reports [32,50–52] indicate that the direct approximation approach to the KS potentials can be a promising route for accurate prediction of static electric polarizabilities, band gaps, and other properties. One such example is the correction introduced by the van Leeuwen and Baerends [34] model to the exchange part of the XC potential. We employ the vLB correction to the LDA exchange as

$$V^{\text{model}}_{xc,\sigma}(\mathbf{r}) = \left[V_{x,\sigma}(\mathbf{r}) + V^{\text{vLB}}_{x,\sigma}(\mathbf{r})\right] + V_{c,\sigma}(\mathbf{r}), \tag{2}$$

where $V_{x,\sigma}(\mathbf{r})$ [$\mathbf{V}_{\mathbf{c},\sigma}(\mathbf{r})$] is the standard LDA exchange [correlation] potential [5] and $V^{\text{vLB}}_{x,\sigma}(\mathbf{r})$ is the correction to the LDA exchange [34]. The suffix σ represents the spin degree of freedom. Here, $V^{\text{vLB}}_{x,\sigma}(\mathbf{r})$ is

$$V^{\text{vLB}}_{x,\sigma}(\mathbf{r}) = -\beta\rho_{\sigma}^{1/3}\frac{x_{\sigma}^{2}}{1+3\beta x_{\sigma}\sinh^{-1}(x_{\sigma})}, \tag{3}$$

where $\beta = 0.05$ was used in the original formulation [34]. The variable $x = |\nabla\rho(\mathbf{r})|/\rho^{4/3}(\mathbf{r})$ signifies the change in the mean electronic distance provided the density is a slowly varying function in a given region with a strong dependence on the gradient of the local radius of the atomic sphere R_{ASA}.

The effective Kohn-Sham potential using Eq. (3) is

$$V_{\text{eff}}(\mathbf{r}) = V_{\text{ext}}(\mathbf{r}) + V_{H}(\mathbf{r}) + \left[V_{x,\sigma}(\mathbf{r}) + V^{\text{vLB}}_{x,\sigma}(\mathbf{r}) + V_{c,\sigma}(\mathbf{r})\right], \tag{4}$$

where the potential contributions are the external $V_{\text{ext}}(\mathbf{r})$, electronic Hartree $V_H(\mathbf{r})$, LDA exchange $V_{x,\sigma}(\mathbf{r})$, LDA correlation $V_{c,\sigma}(\mathbf{r})$, and spin-polarized vLB exchange $V^{\text{vLB}}_{x,\sigma}(\mathbf{r})$. The optimized β, calculated from the IP theorem for atoms and diatoms, helps in calculating accurate densities in solids. This provides us a general procedure for constructing the KS XC potential from a given electron density and produces fairly good asymptotic behavior along with fulfilling the requirements of the EXX potential [34].

The iterative Kohn-Sham scheme now has the effective potential constructed using a new electronic density term:

$$\left\{-\tfrac{1}{2}\nabla^2 + (V_{\text{eff}}(\mathbf{r}) - V_o)\right\}\phi_{i,\sigma}(\mathbf{r}) = (\epsilon_{i,\sigma} - V_o)\phi_{i,\sigma}(\mathbf{r}). \tag{5}$$

In Eq. (5), we call out the potential zero V_o directly, which is arbitrary in the "exact" full-potential linear augmented plane-wave (FLAPW) method but not so in approximate methods. We employ Eq. (5) in the tight-binding, linear muffin-tin orbital (TB-LMTO) method within the atomic sphere approximation (ASA) [53] and obtain the self-consistent solution of the single-particle Schrödinger equation for the vLB-corrected effective potential.

Many site-centered electronic-structure methods, such as LMTO, KKR, and FLAPW, utilize a spherical-harmonic basis within a specified radius and then handle interstitial regions

between atoms at varying levels of accuracy: FLAPW is considered "exact" because it uses thousands of plane waves to represent the unit cell and interstitial. Within the ASA, the atomic spheres are simply increased to conserve the cell volume, while large interstitial voids are represented by nonoverlapping empty spheres (ESs). The ESs contain no ion cores but the associated charge reflects the interstitial potential. Thus, all potentials and eigenenergies are chosen relative to a suitable V_o, which can be set variationally so that the ASA dispersion approaches that of the FLAPW method [54] and establishes the "free-electron"-like behavior inside the crystal (and defines the crystal momentum).

Importantly, LMTO methods, via the tail-cancellation theorem [55], or, equivalently, KKR methods [56,57], through the calculation of the single-site scatterers, permit the vLB correction to be imposed locally for all sites in a multisite (finite or infinite) structure to solve for the collective behavior. That is, the interstitial region within the crystal is effectively the asymptotic region for site-centered methods, where the vLB correction is set at the ASA boundary. Hence, as is typical, we solve the microscopic electrostatic potential inside the crystal, without direct reference to the atomic 0 far outside the crystal.

To connect our results to those of methods that use screened, range-separated hybrid functionals implemented in plane-wave methods, we note that the global reference is set to atomic 0 (far from the atom or far outside the crystal), which requires a dielectric function to solve the macroscopic (long-ranged) electrostatics, as done, for example, by Kronik *et al.* [43–45] In this approach, to set the proper boundary conditions, two of the range-partition variables must obey the sum rule $\alpha + \beta = 1/\epsilon$, where ϵ is the static dielectric function ($\epsilon = 1$ for an atom in vacuum and $1 \leqslant \epsilon \leqslant \infty$ for a crystal). Within our site-centered basis method with potential reference V_o, there is a difference from atomic 0 due to the work function, i.e., $W = -E_F - e\phi$, where $\phi \propto \epsilon$ for systems with a gap. Hence, the present theory should (and does) reproduce the band-gap results of Kronik *et al.* [43–45], without the need to calculate the static dielectric as input. Of course, we can also calculate the W to establish our results relative to atomic 0, for which the long-range Fock and semilocal exchange play a role.

III. COMPUTATIONAL DETAILS

Core states are treated as atomic-like in a frozen-core approximation and energetically higher-lying valence states are addressed in the self-consistent calculations of the effective crystal potential, which is constructed by overlapping Wigner-Seitz spheres for each atom in the unit cell. A twofold criterion for generating the crystal potential, on the same footings as the TB-LMTO-ASA, has been used: (a) use of a trial wave function, i.e., linear combinations of basis functions like plane waves in the nearly free-electron method, and (b) use of a matching condition for partial waves at the sphere boundary [53,58,59].

All spin-polarized vLB-correction calculations were done self-consistently and nonrelativistically for a given experimental geometry until the "averaged relative error" between successive iterations reaches 10^{-5} for the charge density and 10^{-4} for the energy. To facilitate convergence, we have used Anderson mixing. The k-space integration is done using the tetrahedron method with divisions of $12 \times 12 \times 12$ for cubic and $12 \times 12 \times 6$ for noncubic cells along the three primitive reciprocal translation vectors.

Inside the atomic spheres, the Kohn-Sham potential is obtained by using the LDA correlation parameterized by van Barth and Hedin [60] with the corrected EX potential given by Eq. (4), matched at the ASA radii. Following TB-LMTO-ASA requirements [53], the open-shell semiconductor structures are filled with ESs for an improved basis. In empty spheres, given that the absence of a core makes the electron gas reasonably homogeneous and small, the exchange contribution from empty spheres is very small and the correction to the exchange is even smaller; hence, we use the LDA-XC in ESs and implement the vLB correction in atomic spheres only.

The dependence of the dimensionless parameter x present in Eq. (3) on R_{ASA} is very clear from the expression, so the appropriate choice of R_{ASA} is crucial. In all calculations, we chose R_{ASA} by $\pm 5\%$–10% from the default values to control the overlapping of atomic spheres and ESs to reduce the loss of electrons into the (unrepresented) interstitial for open-shell structures, e.g., semiconductors.

In Sec. IV, we have shown that the vLB-corrected LDA provides an accurate band structure for semiconductor and insulators, but due to the absence of the exchange functional E_x such that $\mathrm{V}^{\mathrm{vLB}}_{x,\sigma} = \delta E_x/\delta\rho_\sigma$, we recommend the use of an existing semilocal functional (e.g., LDA or GGA) for the structural properties and then the vLB-corrected LDA to obtain the band structure.

IV. RESULTS AND DISCUSSION

Recently, Hemanadhan *et al.* [48] discussed extensively that the optimal tuning of the parameter β is crucial for achieving an accurate description of the IP theorem for atoms. However, the tuning procedure is challenging in solids because the ionization potential and electron affinity need to be calculated from the total energy differences, a problematic procedure for periodic systems [61]. To achieve this goal, we set a two step criteria: First, we tuned the parameter β for both atom and diatoms to an optimal value using the IP theorem, e.g., we chose the diatom LiF, which has an experimental ionization potential of 11.50 eV. Tuning β to 0.048 from atomic calculations gives $\epsilon^{\beta}_{\mathrm{max}} = -I^{\beta} = 12.17$ eV just 5% from experimental observation. Second, we use the optimal value of $\beta = 0.048$ in the vLB-correction term to the LDA exchange in Eq. (3). In this way, the calculated band gap of LiF using our self-consistent optimized vLB-TB-LMTO-ASA approach is 12.61 eV, which compares well with the 12.60 eV calculated using the range-separated hybrid functional of Refaely-Abramson *et al.* [45] and the experimental value of 13.60 eV [62].

Clearly, adding the vLB correction to the LDA exchange improves the asymptotic behavior over the LDA, and, if used with the optimized-β approach, it satisfies the IP theorem for atoms and diatoms due to its exact density description. Although all quantities used in Eq. (3) are semilocal, they still lead to a good approximation to the EXX type of potentials because of the correct treatment at shell limits, i.e., $r \to 0$ to $r \to R_{\mathrm{ASA}}$. This approach produces good band gaps

TABLE I. Band gaps calculated with the vLB-corrected potential of A1 (fcc) and B1 (rocksalt) systems at values of β satisfying the IP theorem. We compared to results from experiments [13,17–19,62–69], HS-EX, LDA, QPC [70], and MBJ-LDA [31].

		Band gap (eV)					
System	β	vLB	Expt.	HS-EX	LDA	QPC	MBJ
Ne (A1)	0.082	23.64	20.75	22.07	11.39	16.55	22.72
	0.05	23.02					
Ar (A1)	0.058	12.76	14.32	11.29	8.09	11.95	13.91
	0.05	12.46					
Kr (A1)	0.044	10.91	11.40	9.10	6.76	9.98	10.83
	0.05	10.61					
Xe (A1)	0.040	8.61	9.15	6.63	5.56	8.23	8.52
	0.05	8.35					
MgO (B1)	0.070	6.94	7.78	6.23	4.94	–	7.17
	0.05	5.94					
CaO (B1)	0.070	7.15	7.09	7.29	3.36	–	–
	0.05	6.07					
LiF (B1)	0.048	12.61	13.60	9.52	8.94	–	12.94
	0.05	12.31					
LiCl(B1)	0.048	7.84	9.40	6.50	6.06	–	8.64
	0.05		7.85				

for semiconductors and insulators which compare well with experiments [13,17–19,63–69]; see Table I and Fig. 1.

A. Wurtzite-ZnO

A zinc oxide (ZnO) semiconductor remains a topic of interest because of its optoelectronic applications owing to its direct wide band gap, $E_g \sim 3.40$ eV, at room temperature [75]. The ZnO exists in the wurtzite (B4), zinc blende (B3), and rock salt (B1) crystal structures, but under ambient conditions, B4 is thermodynamically the most stable phase. After Rössler's prediction of thr Zn-3d level 12 eV below the valence band maximum in B4-ZnO [76], several experiments [77–80] were

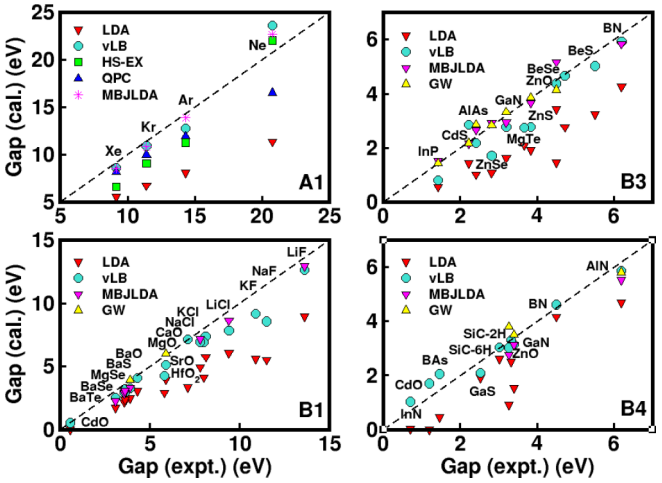

FIG. 1. Band gaps for materials with four structures. Left: A1 (FCC) with $\beta = 0.04$–0.082 and B1 (rock salt) with $\beta = 0.04$–0.08 [71–73]. Right: B3 (zinc blende) with $\beta = 0.03$–0.075 and B4 (wurtzite) with $\beta = 0.03$–0.09 [74].

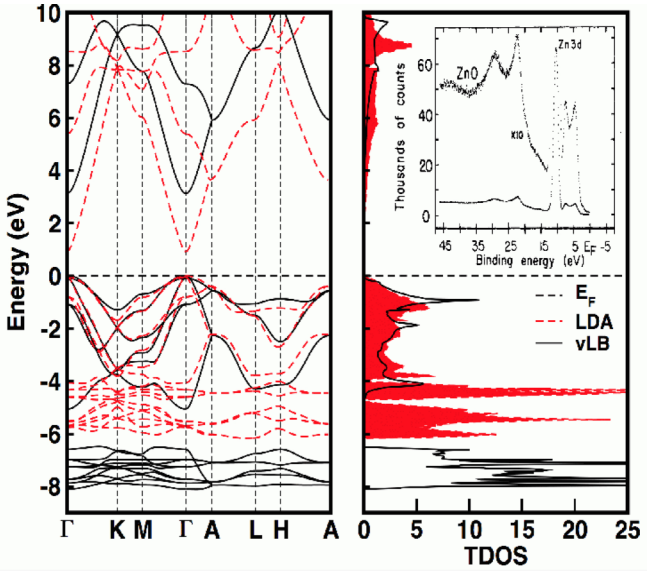

FIG. 2. LDA + vLB results for wurtzite-ZnO give a Zn-3d peak at 7.50 ± 0.2 eV (the LDA is at ~6.0 eV). Inset: The x-ray photoelectron spectrum of the most stable polymorph, i.e., wurtzite-ZnO [80].

done and showed significant differences from the calculated result. Langer *et al.* [77] and Powell *et al.* [78,79] used x-ray-induced photoemission spectroscopy and UV photoemission measurements, respectively, to determine the position of the Zn-3d core level and placed it 7.5 ± 0.2 eV from the valence band maximum: 3 eV lower than that predicted by Rössler. The x-ray photoemission showed similar values to UV, i.e., 8.5 eV by Vesely *et al.* [81] and 8.81 eV by Ley *et al.* [80,82]. Despite the good agreement with the qualitative valence band dispersion from LDA functionals [83–86], the debate on the quantitative position of the Zn-3d level in B4-ZnO remains a good exercise for most semilocal functionals. So, we provide, as one test, results on B4-ZnO from the optimized LDA + vLB potential within the TB-LMTO-ASA.

For ZnO, core and valence orbitals of (Zn, O) were set to ($1s2s2p3s3p3d$, $1s$) and ($4s4p3d$, $2s2p$), respectively. In the calculation of band energies, we use valence states of (Zn, O), i.e., ($4s4p3d$, $2s2p$) as the basis set. We have added two other lattices of empty spheres (ES1, ES2) at [(0,0,0.34), (−0.29,0.5,0.249)] in the unit cell to obtain a close-packed structure fulfilling the criteria needed for the atomic sphere approximation assumed in the TB-LMTO-ASA [53]. Atomic sphere radii, $R_{\rm ASA}$, of (Zn, O) were fixed to (2.095, 1.775) Å in LDA + vLB, HS-EX, and LDA calculations. The basis set used in calculations for [(Zn, O), (E1, E2)] is [($4s4p3d$, $2s2p$), ($1s2p3d$, $1s2p$)] and is complete under all symmetry operations, and no additional basis atom has been introduced.

For the LDA (see Fig. 2), we found Zn-3d levels ~6.0 eV from the Fermi energy E_F, meaning that Zn-3d levels are now incorrectly closer to O-2p states, giving a stronger interaction with O-2p levels. Increased interaction leads to strongly hybridized Zn-3d and O-2p states, which push the O-2p level towards the conduction band minimum, resulting in reduced band gaps. The typical error in estimating ZnO (B4) band gaps using the LDA originated from the strong Coulomb correlations between Zn-3d and O-2p levels. Although exact

calculation of the correlation is not possible, treating the exact exchange is numerically possible. For the optimized LDA + vLB, this is achieved by introducing the vLB correction to the LDA exchange and tuning β to the optimal value through the IP theorem using the atomic constituents. For solid ZnO, the LDA + vLB gives the Zn-3*d* peak center at 7.40 eV, in agreement with measurements, 7.5 ± 0.2 eV. Clearly, the eigenenergies of semicore Zn-3*d* levels (incorrect in the LDA and underestimated with respect to experiments by ~3 eV) are corrected by the introduction of the vLB asymptotic correction introduced here. The band gap of wurtzite-ZnO calculated using the optimized LDA + vLB is ~3.10 eV, which compares well with observed band gap of 3.4 eV [80], while the LDA value is ~1.0 eV (an underestimation of ~71%). The band gaps of wurtzite-ZnO calculated from the optimized vLB versus other methods (MBJLDA [31], HSE06 [87], G0W0 [73], GW [17]) are ~3.10 eV and (2.68 [31], 2.49 [87], 2.51 [73], 3.80 [17]) eV, respectively. Only the optimized-vLB (10% too small) and GW (10% too large) results are in reasonable agreement with experimental values.

B. Half-Heusler alloys

1. *Non-spin-polarized compounds*

In this section, we revisit the work of Kieven *et al.* [88] on I-II-V (eight-electron) half-Heusler systems that have prime importance in optoelectonics. The half-Heusler structure basically arises from three interpenetrating fcc lattices of X, Y, and Z atoms crystallized in ternary XYZ compounds with the $F\bar{4}3m$ space group. The atoms X, Y, and Z are arranged at positions (1/2,1/2,1/2), (0,0,0), and (1/4,1/4,1/4) in units of the cubic lattice parameter and can be viewed as a zinc-blende-like structure. The strongly bound valence electrons in I-II-V half-Heusler compounds separate the conduction and the valence bands, resulting in a semiconducting behavior with varying band gaps [89]. We considered 18 XYZ [X = Li, Na, and K, Y = Mg, Ca, and Zn, and Z = N and P; X, Y, and Z belong to the first (I-A), second (II-A and II-B), and fifth (V-A) main groups (subgroups) of the periodic system of elements] compounds with the half-Heusler structure and calculated band gap (Table II) using the TB-LMTO-ASA with the LDA + vLB potential; in most cases, we find a good agreement in Table II with Kieven *et al.* [88] and experiments [90–93].

TABLE II. Band gaps of I-II-V (B3) half-Heuslers: LDA + vLB with $\beta = 0.05$ (ours), compared to experiment and LDA (ours), as well as GGA, B3LYP, and GW [88,90–93]. All calculations use lattice constants from Kieven *et al.* [88].

	Band gap (eV)					
System	Expt.	vLB	LDA	GGA	B3LYP	GW
LiMgN	3.20	3.37	2.85	2.29	4.37	–
LiMgP	2.43	2.07	1.93	1.55	2.90	–
LiCaN	–	3.71	2.38	2.21	3.78	–
LiCaP	–	2.91	2.23	1.95	–	2.93
LiZnN	1.91	1.67	0.78	0.52	2.34	–
LiZnP	2.04	1.17	1.32	1.35	2.66	–
NaMgN	–	2.72	1.06	0.77	2.08	–
NaMgP	–	2.23	1.54	1.47	2.76	2.79
NaCaN	–	1.82	1.47	1.15	3.03	–
NaCaP	–	1.74	1.01	1.95	–	2.95
NaZnN	–	0.06	0.00	0.00	–	1.83
NaZnP	–	0.00	0.30	0.44	1.64	–
KMgN	–	1.05	0.33	0.13	–	–
KMgP	–	1.25	0.97	0.96	–	–
KCaN	–	2.24	0.82	0.68	2.14	–
KCaP	–	2.08	1.56	1.54	–	2.90
KZnN	–	0.14	0.00	0.00	–	1.98
KZnP	–	0.00	0.00	0.00	–	–

2. *Spin-polarized FeMnSb*

The spin-resolved band structure of half-metallic compounds shows unusual properties: FeMnSb is one example, with a half-Heusler crystal structure discussed thoroughly by de Groot *et al.* [94] and Chioncel *et al.* [95]. To showcase spin-polarized vLB corrections, we consider FeMnSb. The standard representation of FeMnSb with a $C1_b$ crystal structure contains three atoms—Fe(0, 0, 0), Mn(1/4, 1/4, 1/4), and Sb(3/4, 3/4, 3/4)—and a vacant site at (1/2, 1/2, 1/2) (replaced by a chargeless ES for ease in calculations), respectively. In FeMnSb, Fe ($-1\mu_B$) and Mn ($3\mu_B$) moments stabilize the gap and the half-metallic electronic structure with ferrimagnetic coupling with a total moment of $2\mu_B$. The integer spin moment per unit cell criterion is one of the requirements for half-metallicity.

In Fig. 3, electronic states for majority-spin projection have a metallic character with a nonzero density of states at E_F, and states with the minority-spin projection demonstrate a band gap at E_F [94,96]. The gap originates from strong hybridization between the 3*d* states of the transition metals Fe and Mn. This hybridization results in fully bonding states in the valence band and empty antibonding states in the conduction band, leading to a finite gap at E_F (marked by a dashed line at zero energy). The deep-lying *sp* states of Sb do not have much

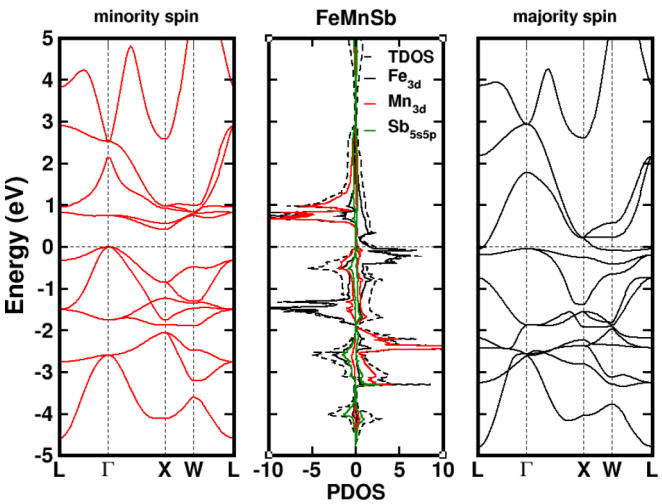

FIG. 3. Spin-resolved band structure of the half-Heusler half-metallic FeMnSb alloy calculated with the LDA + vLB potential at a lattice constant of 5.703 Å [94,95].

TABLE III. Band gaps of boron-nitride and graphene quantum dots (ring sizes 1, 3, and 7) calculated using the LDA + vLB ($\beta = 0.05$) and LDA potentials.

		Band gap (eV)					
Ring size	B-N	Expt.	vLB	LDA	C	vLB	LDA
1	B_3N_3	–	2.00	0.50	C_6	2.90	1.50
3	B_6N_7	–	3.00	1.90	C_{13}	3.46	1.85
7	$B_{12}N_{12}$	–	5.70	2.40	C_{24}	5.20	2.50
Bulk	h-BN	3.60–5.90 [112,113]	4.60	3.90	–	–	–

effect on the density of states at E_F, so it is not responsible for the existence of the minority gap. As a result, half-metal can, in principle, conduct a fully spin-polarized current, and hence it attracts attention for potential spintronics applications [96,97].

C. Quantum dots: Boron nitride and graphene

Two-dimensional materials, like graphene and hexagonal boron nitride (h-BN), have drawn tremendous attention in terms of both fundamental physics and possible applications in energy-generation devices [98–100]. Single layers of graphene and h-BN have been fabricated and found to be stable at room temperature [101–105]. The electrical conductivity in both cases varies largely because graphene is a semimetal and a very good conductor, while BN is an insulator (band gap ~6 eV) [106,107].

We modeled ring size 1 (3 B + 3 N or 6 C atoms), ring size 3 (6 B + 7 N or 13 C atoms), and ring size 7 (12 B + 12 N or 24 C atoms) quantum dots of boron nitride and graphene within a cell of orthorhombic symmetry with cell parameters $a = c = 40$ Å and $b = 25$ Å. The experimental geometry is used to generate two-dimensional quantum dots [108,109].

We calculated the LDA and LDA + vLB gaps between HO molecular orbitals and LU molecular orbitals (LUMOs) of boron-nitride dots, where boron and nitrogen have (3,3), (6,7), and (12,12) atoms each in the basis sets. Because the TB-LMTO uses the ASA, we fill the rest of the cell volume with ESs and include them in the basis set along with the atoms. As reported in Table III, with increasing dot size we approach the bulk optical band gap. The LDA + vLB potential within the TB-LMTO-ASA yields a HOMO-LUMO gap of 5.70 eV for $B_{12}N_{12}$ (Table III), which compares reasonably to the bulk band gaps observed (3.6 eV [112] and 5.9 eV [113]) and predicted (2.45 eV [110] to 5.4 eV [111]), while the LDA largely underestimates all values.

V. CONCLUSION

Since KS-DFT was first proposed, the search has remained unabated for a quality but numerically fast exchange-correlation functional to predict band gaps correctly. Here, we have presented results using a spin-polarized vLB-corrected potential, which matched the asymptotic behavior of exchange at the atomic sphere boundary (i.e., local interstitial in the solid) and which also satisfied the ionization potential theorem for atomic constituents. The combination approximately enforces that the ionization energy and HOMO-LUMO difference agree in first-principle calculations. The LDA + vLB–corrected exchange in combination with the IP theorem may be a good candidate for filling the gap of orbital-dependent functionals using semilocal quantities, and it provides an approximate exact-exchange band structure with no more computational cost than the LDA or GGA. Compared with experiments, our asymptotically corrected LDA obtains accurate band gaps for semiconductors and insulators, where in some cases it yields gaps comparable to or better than those obtained with more sophisticated XC methods, such as the hybrid, exact exchange, and GW.

ACKNOWLEDGMENTS

We thank A. Alam (Indian Institute of Technology, Mumbai, India) and W. A. Shelton (Louisiana State University, Baton Rouge) for critical comments. Work at Ames Laboratory was supported by the U.S. Department of Energy (DOE), Office of Science, Basic Energy Sciences, Materials Science and Engineering Division. The research was performed at the Ames Laboratory, which is operated for the U.S. DOE by Iowa State University under Contract No. DE-AC02-07CH11358. D.D.J. also acknowledges support from a U.S. DOE "Computational Materials Science Network" grant through Brookhaven National Laboratory.

[1] S. Kümmel and L. Kronik, Rev. Mod. Phys. **80**, 3 (2008).
[2] V. Sahni, *Quantal Density Functional Theory* (Springer, Berlin, 2004).
[3] P. Hohenberg and W. Kohn, Phys. Rev. **136**, B864 (1964).
[4] W. Kohn and L. J. Sham, Phys. Rev. **140**, A1133 (1965).
[5] J. P. Perdew and Y. Wang, Phys. Rev. B **45**, 13244 (1992).
[6] J. P. Perdew, J. A. Chevary, S. H. Vosko, K. A. Jackson, M. R. Pederson, D. J. Singh, and C. Fiolhais, Phys. Rev. B **46**, 6671 (1992).
[7] J. P. Perdew, A. Ruzsinszky, G. I. Csonka, O. A. Vydrov, G. E. Scuseria, L. A. Constantin, X. Zhou, and K. Burke, Phys. Rev. Lett. **100**, 136406 (2008).
[8] J. Perdew, Chem. Phys. Lett. **64**, 127 (1979).
[9] M. R. Pederson and C. C. Lin, J. Chem. Phys. **88**, 1807 (1988).
[10] J. P. Perdew and A. Zunger, Phys. Rev. B **23**, 5048 (1981).
[11] V. I. Anisimov, J. Zaanen, and O. K. Andersen, Phys. Rev. B **44**, 943 (1991).
[12] W. G. Aulbur, M. Stadele and A. Gorling, Phys. Rev. B **62**, 7121 (2000).
[13] S. V. Faleev, M. van Schilfgaarde, and T. Kotani, Phys. Rev. Lett. **93**, 126406 (2004).
[14] M. van Schilfgaarde, T. Kotani, and S. V. Faleev, Phys. Rev. B **74**, 245125 (2006).
[15] A. N. Chantis, M. van Schilfgaarde, and T. Kotani, Phys. Rev. B **76**, 165126 (2007).
[16] M. Shishkin and G. Kresse, Phys. Rev. B **75**, 235102 (2007).

[17] M. Shishkin, M. Marsman, and G. Kresse, Phys. Rev. Lett. **99**, 246403 (2007).
[18] J. Heyd, J. E. Peralta, G. E. Scuseria, and R. L. Martin, J. Chem. Phys. **123**, 174101 (2005).
[19] J. Paier, M. Marsman, K. Hummer, G. Kresse, I. C. Gerber, and J. G. Angyan, J. Chem. Phys. **124**, 154709 (2006); **125**, 249901 (2006).
[20] J. P. Perdew, R. G. Parr, M. Levy, and J. L. Balduz Jr., Phys. Rev. Lett. **49**, 1691 (1982).
[21] L. J. Sham and M. Schlüter, Phys. Rev. Lett. **51**, 1888 (1983).
[22] J. P. Perdew and M. Levy, Phys. Rev. Lett. **51**, 1884 (1983).
[23] D. J. Tozer, J. Chem. Phys. **119**, 12697 (2003).
[24] M. E. Casida, C. Jamorski, K. C. Casida, and D. R. Salahub, J. Chem. Phys. **108**, 4439 (1998).
[25] E. Kraisler and L. Kronik, J. Chem. Phys. **140**, 18A540 (2014).
[26] T. Grabo, T. Kreibich, and E. K. U. Gross, Mol. Eng. **7**, 27 (1997).
[27] E. Engel and R. Dreizler, *Density Functional Theory: An Advanced Course* (Springer, Berlin, 2011).
[28] T. Kotani, Phys. Rev. Lett. **74**, 2989 (1995); Phys. Rev. B **50**, 14816 (1994).
[29] A. D. Becke and E. R. Johnson, J. Chem. Phys. **124**, 221101 (2006).
[30] F. Tran, P. Blaha, and K. Schwarz, J. Phys.: Condens. Matter **19**, 196208 (2007).
[31] F. Tran and P. Blaha, Phys. Rev. Lett. **102**, 226401 (2009).
[32] M. Kuisma, J. Ojanen, J. Enkovaara, and T. T. Rantala, Phys. Rev. B **82**, 115106 (2010).
[33] R. Armiento and S. Kümmel, Phys. Rev. Lett. **111**, 036402 (2013).
[34] R. van Leeuwen and E. J. Baerends, Phys. Rev. A **49**, 2421 (1994).
[35] C. J. Umrigar, K. G. Wilson, and J. W. Wilkins, Phys. Rev. Lett. **60**, 1719 (1988).
[36] C. J. Umrigar and X. Gonze, Phys. Rev. A **50**, 3827 (1994).
[37] M. K. Y. Chan and G. Ceder, Phys. Rev. Lett. **105**, 196403 (2010).
[38] M. K. Harbola and V. Sahni, Phys. Rev. Lett. **62**, 489 (1989); V. Sahni and M. K. Harbola, Int. J. Quantum Chem. Symp. **38**, 569 (1990).
[39] P. Singh, M. K. Harbola, B. Sanyal, and A. Mookerjee, Phys. Rev. B **87**, 235110 (2013).
[40] P. Singh, M. K. Harbola, and A. Mookerjee, *Modeling, Characterization, and Production of Nanomaterials*, 1st ed., edited by V. K. Tewary and Y. Zhang (Woodhead, Waltham, MA, 2015), Vol. 1, pp. 407–418.
[41] A. D. Becke, Phys. Rev. A **38**, 3098 (1988).
[42] C. O. Almbladh and U. von Barth, Phys. Rev. B **31**, 3231 (1985).
[43] I. C. Gerber, J. G. Ángyán, M. Marsman, and Kresse, J. Chem. Phys. **127**, 054101 (2007).
[44] S. Refaely-Abramson, S. Sharifzadeh, M. Jain, R. Baer, J. B. Neaton, and L. Kronik, Phys. Rev. B **88**, 081204(R) (2013).
[45] S. Refaely-Abramson, M. Jain, S. Sharifzadeh, J. B. Neaton, and L. Kronik, Phys. Rev. B **92**, 081204(R) (2015).
[46] T. Stein, H. Eisenberg, L. Kronik, and R. Baer, Phys. Rev. Lett. **105**, 266802 (2010).
[47] I. Dabo, A. Ferretti, N. Poilvert, Y. Li, N. Marzari, and M. Cococcioni, Phys. Rev. B **82**, 115121 (2010); S. Lany and A. Zunger, *ibid.* **80**, 085202 (2009).
[48] M. Hemanadhan, M. Shamim, and M. K. Harbola, J. Phys. B: At. Mol. Opt. Phys. **47**, 115005 (2014).
[49] S. H. Vosko, L. Wilk, and M. Nusair, Can. J. Phys. **58**, 1200 (1980).
[50] R. Armiento, S. Kümmel, and T. Körzdörfer, Phys. Rev. B **77**, 165106 (2008).
[51] A. Karolewski, R. Armiento, and S. Kümmel, J. Chem. Theory Comput. **5**, 712 (2009).
[52] D. Koller, F. Tran, and P. Blaha, Phys. Rev. B **83**, 195134 (2011).
[53] O. Jepsen and O. K. Andersen, *The Stuttgart TB-LMTO-ASA Program, Version 4.7* (Max-Planck-Institut für Festkörperforschung, Stuttgart, Germany, 2000).
[54] A. Alam and D. D. Johnson, Phys. Rev. B **85**, 144202 (2012).
[55] H. Skriver, *The LMTO Method*, Springer Series in Solid-State Sciences, Vol. 41 (Springer, Heidelberg, 1983).
[56] J. Korringa, Physica **13**, 392 (1947).
[57] W. Kohn and N. Rostoker, Phys. Rev. **94**, 1111 (1954).
[58] O. K. Andersen, Phys. Rev. B **12**, 3060 (1975); in *The Electronic Structure of Complex Systems*, edited by P. Phariseau and W. M. Temmerman (Plenum Press, New York, 1984).
[59] O. K. Andersen, O. Jepsen, and M. Sob, in *Electronic Band Structure and Its Applications*, edited by M. Yussouff (Springer-Verlag, Berlin, 1986).
[60] U. van Barth and L. Hedin, J. Phys. C: Solid State Phys. **15**, 1629 (1972).
[61] V. Vlček, H. R. Eisenberg, G. Steinle-Neumann, L. Kronik, and R. Baer, J. Chem. Phys. **142**, 034107 (2015).
[62] P. O. Löwdin, Adv. Phys. **5**, 1 (1956).
[63] R. J. Magyar, A. Fleszar, and E. K. U. Gross, Phys. Rev. B **69**, 045111 (2004).
[64] M. Rohlfing and S. G. Louie, Phys. Rev. B **62**, 4927 (2000).
[65] S. Hufner, J. Osterwalder, T. Riesterer, and F. Hulliger, Solid State Commun. **52**, 793 (1984).
[66] G. A. Sawatzky and J. W. Allen, Phys. Rev. Lett. **53**, 2339 (1984).
[67] M. Marsman, J. Paier, A. Stroppa, and G. Kresse, J. Phys. Condens. Matter **20**, 064201 (2008).
[68] U. Rössler, Phys. Status Solidi B **42**, 345 (1970); in *Rare-Gas Solids*, edited by M. L. Klein and J. A. Venables (Academic Press, New York, 1975), p. 545.
[69] *Semiconductor: Other than Group IV Elements and III-V Compounds*, edited by O. Madelung and R. Poerschke (Springer, Berlin, 1992).
[70] N. C. Bacalis, D. A. Papaconstantopoulos, and W. E. Pickett, Phys. Rev. B **38**, 6218 (1988).
[71] H. Dixit, D. Lamoen, and B. Partoens, J. Phys.: Condens. Matter **25**, 035501 (2013).
[72] P. D. C. King, T. D. Veal, A. Schleife, J. Zúñiga-Pérez, B. Martel, P. H. Jefferson, F. Fuchs, V. Muñoz-Sanjosé, F. Bechstedt, and C. F. McConville, Phys. Rev. B **79**, 205205 (2009).
[73] M. van Schilfgaarde, T. Kotani, and S. Faleev, Phys. Rev. Lett. **96**, 226402 (2006).
[74] B. Wenzien, P. Kackell, F. Bechstedt, and G. Cappellini, Phys. Rev. B **52**, 10897 (1995).
[75] D. Vogel, P. Krüger, and J. Pollmann, Phys. Rev. B **52**, R14316(R) (1995).
[76] U. Rössler, Phys. Rev. **184**, 733 (1969).

[77] D. W. Langer and C. J. Vesely, Phys. Rev. B **2**, 4885 (1970).

[78] R. A. Powell, W. E. Spicer, and J. C. McMenamin, Phys. Rev. Lett. **27**, 97 (1971).

[79] R. A. Powell, W. E. Spicer, and J. C. McMenamin, Phys. Rev. B **6**, 3056 (1972).

[80] L. Ley, R. A. Pollak, F. R. McFeely, S. P. Kowalezyk, and D. A. Shirley, Phys. Rev. B **9**, 600 (1974).

[81] C. J. Vesely, R. L. Hengehold, and D. W. Langer, Phys. Rev. B **5**, 2296 (1972).

[82] Ü. Özgür, Ya. I. Alivov, C. Liu, A. Teke, M. A. Reshchikov, S. Doğan, V. Avrutin, S.-J. Cho, and H. Morkocd, J. Appl. Phys. **98**, 041301 (2005).

[83] S. Bloom and I. Ortenburger, Phys. Status Solidi B **58**, 561 (1973).

[84] J. R. Chelikowsky, Solid State Commun. **22**, 351 (1977).

[85] I. Ivanov and J. Pollmann, Phys. Rev. B **24**, 7275 (1981).

[86] D. H. Lee and J. D. Joannopoulos, Phys. Rev. B **24**, 6899 (1981).

[87] F. Oba, A. Togo, I. Tanaka, J. Paier, and G. Kresse, Phys. Rev. B **77**, 245202 (2008).

[88] D. Kieven, R. Klenk, S. Naghavi, C. Felser, and T. Gruhn, Phys. Rev. B **81**, 075208 (2010).

[89] C. Kandpal, C. Felser, and R. Seshadri, J. Phys. D **39**, 776 (2006).

[90] K. Kuriyama and T. Katoh, Phys. Rev. B **37**, 7140 (1988).

[91] K. Kuriyama, T. Kato, and T. Tanaka, Phys. Rev. B **49**, 4511 (1994).

[92] K. Kuriyama, K. Kushida, and R. Taguchi, Solid State Commun. **108**, 429 (1998).

[93] K. Kuriyama, K. Nagasawa, and K. Kushida, J. Cryst. Growth **237**, 2019 (2002).

[94] R. A. de Groot, F. M. Mueller, P. G. van Engen, and K. H. J. Buschow, Phys. Rev. Lett. **50**, 2024 (1983).

[95] L. Chioncel, E. Arrigoni, M. I. Katsnelson, and A. I. Lichtenstein, Phys. Rev. Lett. **96**, 137203 (2006).

[96] V. Yu. Irkhin and M. I. Katsnelson, Usp. Fiz. Nauk **164**, 705 (1994); Phys. Usp. **37**, 659 (1994).

[97] I. Žutić, J. Fabian, and S. D. Sarma, Rev. Mod. Phys. **76**, 323 (2004).

[98] A. H. C. Neto, F. Guinea, N. M. R. Peres, K. S. Novoselov, and A. K. Geim, Rev. Mod. Phys. **81**, 109 (2009).

[99] A. K. Geim and K. S. Novoselov, Nat. Mater. **6**, 183 (2007).

[100] D. Golberg, Y. Bando, Y. Huang, T. Terao, M. Mitome, C. Tang, and C. Zhi, ACS Nano **4**, 2979 (2010).

[101] K. S. Novoselov, D. Jiang, F. Schedin, T. J. Booth, V. V. Khotkevich, S. V. Morozov, and A. K. Geim, Proc. Natl. Acad. Sci. USA **102**, 10451 (2005).

[102] J. C. Meyer, A. K. Geim, M. I. Katsnelson, K. S. Novoselov, T. J. Booth, and S. Roth, Nature **446**, 60 (2006).

[103] M. H. Gass, U. Bangert, A. L. Bleloch, P. Wang, R. R. Nair, and A. K. Geim, Nat. Nanotechnol. **3**, 676 (2008).

[104] C. Jin, F. Lin, K. Suenaga, and S. Iijima, Phys. Rev. Lett. **102**, 195505 (2009).

[105] A. Nag, K. Raidongia, K. P. S. S. Hembram, R. Datta, U. V. Waghmare, and C. N. R. Rao, ACS Nano **4**, 1539 (2010).

[106] P. R. Wallace, Phys. Rev. **71**, 622 (1947).

[107] X. Blase, A. Rubio, S. G. Louie, and M. L. Cohen, Phys. Rev. B **51**, 6868 (1995).

[108] L. G. Carpenter and P. Y. Kirby, J. Phys. D **15**, 1143 (1982).

[109] V. L. Solozhenko, G. Will, and F. Elf, Solid State Comm. **96**, 1 (1995).

[110] M. S. Nakhmanson and V. P. Smirnov, Fiz. Tverd. Tela **13**, 3788 (1971) [Sov. Phys.-Solid State **13**, 752 (1971); **13**, 2763 (1972)].

[111] E. Doni and G. P. Parravicini, Nuovo Cimento A **63**, 117 (1969).

[112] V. A. Fomichev, Fiz. Tverd. Tela **13**, 907 (1971) [Sov. Phys.-Solid State **13**, 754 (1971)].

[113] W. Baronian, Mater. Res. Bull. **7**, 119 (1972).